Bovine serum albumin and sodium hyaluronate adsorption onto titanium nitrides

Carlos Completo

Centro de Química Estrutural, Instituto Superior Técnico, Av. Rovisco Pais, 1049-001 Lisboa, Portugal

October 2008

Abstract

The use of hard coatings in medical implants is a strategy used to improve performance and lifetime of medical devices. Host response and tribological performance of the surface depend on the contact between the biological fluids and the implant. Albumin and hyaluronic acid are two of the major components present in synovial fluid. The aim of this work was to study bovine serum albumin (BSA) and sodium hyaluronate (NaHA) adsorptions, at 25ºC, onto three ceramic hard coatings deposited by physical vapor deposition (PVD): titanium nitride (TiN), titanium-niobium nitride (TiNbN) and titanium carbonitride (TiCN). The techniques used in the adsorption study were the quartz crystal microbalance with dissipation analysis (QCM-D) and the atomic force microscopy (AFM). In the analyzed BSA concentration range, the results obtained show that there are no significant differences between adsorption on the three coatings although it is observed a trend of more adsorption in TiN followed by TiNbN and TiCN. We can even admit that adsorbed BSA forms a monolayer because the determined film thicknesses are comparable with the molecular dimensions. It was shown that NaHA adsorbs on TiNbN and that simultaneous adsorption of BSA and NaHA leads to similar results than single BSA adsorption. In the sequential adsorption of NaHA to the BSA monolayer no increase in the adsorbed mass was detected and therefore we can conclude that interaction of NaHA with BSA is weak at neutral pH. The adhesion forces between TiN-BSA, TiNbN-BSA and BSA-BSA pairs were determined by force versus distance curves obtained by AFM. Experimental results confirm the drop in adhesion force when BSA is present on both surfaces.

Keywords: Albumin; Hyaluronic Acid; Adsorption; Quartz Crystal Microbalance; Atomic Force Microscopy; Titanium Nitride

1. Introduction

Every year more than 1.5 million hip and knee prostheses are implanted worldwide with a 10 year success rate of more than 90%, [1,2]. Unfortunately, in many active patients prostheses degradation and tissue inflammation are the result of wear particles due articulation friction.

In recent decades prostheses are typically built with a metal or ceramic part articulating against an ultra high molecular weight polyethylene (UHMWPE) part. However, this typology results in heavy wear rate between 100 and 200 μm/year. Alternative materials are metal-on-metal and ceramic-on-ceramic pairs with 5 μm/year wear rates. Ceramics like alumina and zirconia have high fracture rates compared with other materials which are a major limitation in their use.

There are two main future directions in prosthetic materials enhancement: development of coatings for metal substrates and improvement of ceramics properties.

Recent "in vitro" studies showed that titanium ceramics like TiN, TiCN and TiNbN have better friction and wear performance and higher hardness (Table 1), [3], compared with traditional metallic alloys (stainless steel, cobalt-chromium alloys and titanium alloys), [4,5]. However monolayer coatings result in long term wear probably due to high interfacial tensions between the substrate and the coating, as shown in "in vivo" prostheses after extraction from patients. Recent developments on coatings technology, using multilayer or gradient layers which have low interfacial tension, may overcome this problem.

On the other hand, it was demonstrated that lubricant properties of the synovial fluid depend on the presence of albumin and hyaluronic acid. This justifies the relevance of the study of the adsorption of these two molecules on titanium ceramic surfaces, [6-8].

Table 1 – Hardness, H, and Young's Modulus, E, in several materials.

Coating	H (GPa)	E (GPa)
TiN	8.2 – 29	170 – 298
TiCN	11.8 – 38	182 – 199
TiNbN	30 – 51	n.d.
Steel (316L)	2.0 – 6.7	190
Ti	2.4 – 4.4	110 - 169
Ti6Al4V	6.0 – 9.2	116

The aim of this work was to study BSA and NaHA adsorption on three titanium nitrides with a quartz crystal microbalance with dissipation (QCM-D) and atomic force microscopy (AFM). With QCM-D we can determine mass adsorption and the viscoelastic properties of the adsorbed layer, while AFM leads to surface topography and adhesion forces.

2. Theory and background

Performance of the implants depends on its mechanical properties but also on host's response, which begins after the implantation with the adsorption of macromolecules present in the biological fluids.

Protein adsorption, although undesirable in some cases like the formation of blood thrombos, plays an important role in cellular adhesion, for example in osseointegration, and in the improvement of the tribological behavior of articulating joints.

Adsorption is a complex process that consists in three main steps: approaching, attachment and relaxation. Convective and diffusive transport constitute the approaching step and, when the distance to surface is less than 1 μm, interfacial forces (solvatation, electrostatic and Van der Waals) are responsible for the attachment. At the surface, proteins can undergo processes like desorption, surface diffusion, relaxation and conformational changes.

The equilibrium relationship, at constant temperature, between amount of the species adsorbed at the surface and in solution is called "adsorption isotherm".

Several theoretical models can be used to describe the experimental results. The most common models are Langmuir and Freundlich models defined, for adsorption of a single species, in equations 1 and 2, [9]:

$$\Gamma = \frac{\Gamma_\infty \cdot K_L \cdot C}{1 + K_L \cdot C} \tag{1}$$

$$\Gamma = K_F \cdot C^{1/n_F} \tag{2}$$

where Γ is the equilibrium adsorbed amount, also known as superficial concentration, and C is the equilibrium concentration in the solution. The adsorbed amount in a limit monolayer, Γ_∞, and the other model parameters, K_L, K_F and n_F are obtained by linearization of equations 1 and 2.

In the adsorption of a single species, K_L is equivalent to the adsorption equilibrium constant and the free Gibbs energy can be obtained by, [10]:

$$K_L = \frac{1}{c_{solv.}} \exp\left(\frac{\Delta G_{ads.}}{RT}\right) \tag{3}$$

where R is the gas constant, T the temperature and $c_{solv.}$ is the solvent concentration. At dilute concentrations we admit $c_{solv.} = 55.5$ mol/L.

Adsorption isotherms can be obtained experimentally, monitoring adsorbed amount at real time, by techniques like QCM-D, ellipsometry, and surface plasmon resonance (SPR).

QCM-D technique consists in monitoring the variation of the vibration frequency of quartz crystal, Δf, since it is admitted a direct proportionality between Δf and mass variation (adsorbed mass), Δm. For thickness shear mode (TSM) quartz crystals, under vacuum and rigid film adsorption, this proportionality is defined by Sauerbrey equation, [11]:

$$\Delta m = -\Delta f \cdot C_S \tag{4}$$

where the C_S constant can be expressed as, [12]:

$$C_S = \frac{\rho_q \cdot t_q}{f_0} = \frac{\rho_q \cdot v_q}{2f_0^2} = \frac{\sqrt{\rho_q \cdot \mu_q}}{2f_0^2} \tag{5}$$

where f_0 is the quartz crystal fundamental resonance frequency and ρ_q, t_q, μ_q and v_q and are, respectively, the quartz density, thickness, elasticy and shear wave velocity.

At higher frequency harmonic, n, Sauerbrey equation can be generalized by, [13]:

$$\Delta m = -\Delta f \cdot \frac{C_S}{n} \tag{6}$$

When we can not assume that deposited layer has a rigid behavior the adsorbed mass should be estimated by modified Sauerbrey equation, [14]:

$$\Delta m = -\Delta f \cdot \frac{C_S}{n} \cdot \lambda \tag{7}$$

The correction coefficient, λ, is defined by:

$$\lambda = \frac{1}{\left(1 - \omega \rho_l \eta_l \frac{J_f''}{\rho_f}\right)} \tag{8}$$

and J_f'' are defined by:

$$J_f'' = \frac{\omega \eta_f}{\mu_f^2 + \omega^2 \eta_f^2} \tag{9}$$

where ω is the angular vibration frequency, ρ_l is the liquid density, η_l is the liquid viscosity, ρ_f is the film density, η_f is the film viscosity and μ_f is the film elasticity.

The viscoelastic properties of the adsorbed film layer are obtained from equipment analysis software which uses Voigt model to fit to the experimental results, [13].

Titanium and titanium ceramics surfaces are covered with natural oxide layers and their surface chemical composition can be determined by x-ray photoelectron spectroscopy (XPS). In XPS technique, [15], the sample is bombarded with x-ray radiation and ejected electrons are counted. Each element has typical binding energies and these are influenced by neighbor atoms. In this way it is possible to identify and to quantify surface chemical composition

Other important parameters to characterize surfaces are the average roughness, R_a, and the peak-to-valley height, R_{pV}, which are defined by, [16]:

$$R_a = \frac{1}{L}\int_0^L |y(x)|dx \quad (10)$$

$$R_{pV} = \{(\text{maximum sample height}) - (\text{minimum sample height})\} \quad (11)$$

where L is the length of the profile, x is the distance to origin in x axis and y is the height difference between height at position x and average height.

These surface topographic parameters were determined by AFM. The AFM technique consists of a microscale cantilever with a sharp tip (probe) at its end that is used to scan the specimen surface (see Figure 1), [17].

AFM imaging can be done in two modes: contact and dynamic mode.

In contact mode the forces are repulsive and when the tip is brought into proximity of a sample surface, forces between the tip and the sample lead to a deflection of the cantilever according to Hooke's law. This deflection is converted in surface topography.

In dynamic mode the cantilever oscillates near its resonant frequency and the oscillation amplitude, phase and resonance frequency are modified by tip-sample interaction forces. These changes in oscillation provide information about the characteristics of the samples.

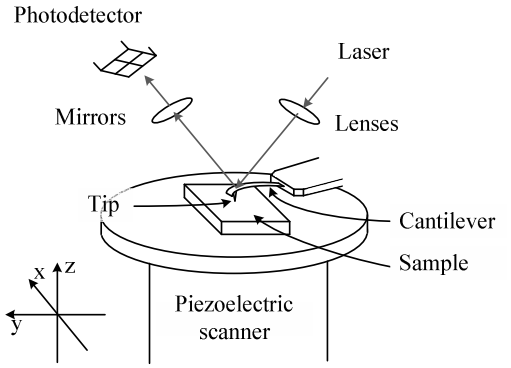

Figure 1 – AFM aparatus.

With AFM technology we can also determine the adhesion force between two surfaces, F_{ad}. This technique consists in approaching and retracting a tip against the sample and obtaining force measurements from deflection of the cantilever. One of the most important interaction force between two bodies is Van der Waals force which for the interaction between a plane surface and a sphere can be estimated by, [18]:

$$F_{ad} = \frac{A_H R}{6D^2} \quad (12)$$

where R is the sphere's radius, D is an interatomic spacing often assumed as 0.165 nm and A_H is the Hamaker constant of the system in study.

3. Experimental procedure

3.1 Materials

Uncoated stainless steel 316L plates (1x1 mm) and discs (Ø = 10 mm) were used in XPS and AFM analyses. Quartz crystal resonator discs (Ø = 14 mm) coated with gold provided by KSV Instruments Ltd. were used in QCM studies.

All substrates and coated surfaces were cleaned in an ultrasonic bath with Extran diluted solution (10% v/v) for 10 min and rinsed with distilled and deionised water from Milli-Q. The cleaning procedure used for the surfaces incubated with BSA and/or NaHA was sonication in sodium dodecyl sulfate (3%, from Sigma-Aldrich) followed by rinsing with Milli-Q, and finally blowing dry with nitrogen.

Hank's balanced salt solution - HBSS (Sigma, ref. H8264), bovine serum albumin - BSA (Serva, ref. 11930) and sodium hyalurunate – NaHA (Fluka, ref. 53747) were used to prepare the solutions.

3.2 Methods

Substrates coating and polishing

The coatings were deposited by arc evaporation physical vapor deposition with a METAPLAS coating machine, at 300ºC. The samples were etched with titanium ions at 900 V bias voltage to remove any possible oxide on the surface. In the deposition process the following parameters were used: 200 A cathode deposition current; 100 V bias voltage and $1.4x10^{-2}$ mbar for the gas pressure. A Ti cathode was used for TiN and TiCN, and a cathode of TiNb alloy, for TiNbN. TiN and TiNbN were produced under nitrogen atmosphere. For TiCN, besides nitrogen, also acetylene was introduced.

Some coated discs used in AFM were polished in a Wazau TRM1000 tribometer controlled by TriboV4 version 4.1 software. Polishing was carried out during 7 minutes with a normal load of 30 N and a tangential sliding velocity of 142 mm/s for TiN coatings and during 26 minutes with a normal load of 15 N and a tangential sliding velocity of 90 mm/s for TiNbN and TiCN.

XPS

X-ray photoelectron spectroscopy (XPS) was performed using a Microlab 310F system (VG Scanning). The spectra were obtained at a pressure of $5 \cdot 10^{-9}$ mbar using X-ray from a Mg Ka source (15 kV / 20 mA). Chemical identification and determination of relative atomic concentrations were based on individual ionizations obtained with a passing energy of 30 eV. The photoelectrons were analyzed at the takeoff angle of 30º. The elemental sensitivity factors were obtained from the VG databank. All the peaks positions were referenced to carbon 1s orbital at 285.0±0.2 eV. Numerical fitting of the spectra was made using a Gaussian-Lorenzian algorithm. The deconvolution of the peaks was based on reported binding energies, [19-22]. It were analyzed two plates of each titanium ceramic.

QCM

The quartz crystal microbalance with dissipation (KSV Instruments Ltd, Finland, model QCM-Z500) was used to determine BSA adsorption on the surface of the quartz crystals coated with TiN, TiCN and TiNbN.

In order to avoid possible surface contaminations, all the QCM parts of the measuring cell were sonicated in Extran diluted solution, rinsed in Milli-Q water, and blown dry with nitrogen.

The fundamental frequency along with the third, fifth, seventh, ninth and eleventh harmonics were monitored as a function of time to determine the changes in frequency upon the sequential addition of HBSS, BSA and/or NaHA solutions and HBSS, to the quartz crystal. The dissipation change was also recorded along the process. The experiments were performed at 25ºC. At least three independent measurements were done for each concentration.

Considering the baseline for the first addition of HBSS, the subsequent changes correspond to the formation of a BSA/NaHA layer on the surface of the crystal followed by a weak removal of adsorbed molecules during rinsing with the solvent. When the viscoelastic properties of the adsorbed film can not be neglected, there are four unknown parameters when modeling the properties of the adsorbed layer, namely thickness, density, elasticity and viscosity. The QCM-D software (QCM-Z500 Data analyzer, version 1.62) based on the surface mechanical impedance model allows to model thickness, viscosity and elasticity for a viscoelastic layer whose density is known. Assuming the value of 1.15 g/cm^3 for the density of the adsorbed BSA film, [23], the remaining parameters were calculated.

AFM

A VeecoTM DI CP-II atomic force microscope was used for the topographic characterization and force spectroscopy. Silicon etched probes (MPP111 and MPP311 models from Veeeco), with a nominal radius of 10 nm and a nominal constant of 40 N/m and 0.9 N/m, respectively, were used for topographic imaging. Substrate surface dry imaging was done with MPP311 probes in contact mode at room humidity and temperature conditions while the film imaging under water was performed in non-contact mode with MPP311 probes. The average roughness, Ra, of the disks was measured over 10x10 μm^2, 30x30 μm^2 and 136x136 μm^2 areas.

To estimate the protein film thickness, the samples were tested under water to avoid protein denaturation using a liquid MicroCell. First, the protein film was removed by performing two scans in contact mode on areas of 2x2 μm^2. These scans were made with a scan rate of 1 Hz, a resolution of 512 lines and a load of 9 μN. This load was found to be sufficient to remove most of the protein film on the surface without any damage of the underlying substrate. Immediately after, 4x4 μm^2 scans were performed with the same probe over the cleaned area, in non-contact mode, in order to visualize the surface.

The thickness of the films was measured on mean profiles for each scar, considering an average flat reference surface. The position of this reference surface was assumed to be the middle value of the surface asperities height distribution function, retrieved from the surface topographical profile in the region outside the scar.

The preparation of the adsorbed albumin films was carried out by immersion of the samples in the HBSS+BSA solution (10 mg/mL) during 1 hour, at room temperature. After immersion, the samples were rinsed with water to remove unbound protein and transferred to the liquid cell without drying.

4. Results and discussion

4.1 Surface characterization of titanium ceramics

Surface chemical composition of the three titanium ceramics were determined by XPS analyses (Table 2).

Table 2 – Surface elemental chemical composition (%).

	TiN	TiNbN	TiCN
Ti	30.7	22.8	27.1
N	20.8	20.6	10.3
O	34.1	38.0	41.0
C	14.4	11.5	21.6
Nb	-	7.2	-
Total	100.0	100.0	100.0

The XPS peak deconvolution ranges of the analyzed samples are shown in Table 3. The comparison of the experimental results with the existing literature allow us to identify the corresponding chemical bond of each band (Table 3), [19-22]. Besides natural oxide, other contribution to oxygen band derives from the presence of adsorbed water and organic contaminations. These contaminations are also the explanation of the presence of carbon in samples where it was not supposed to be present like TiN and TiNbN.

Table 3 – XPS deconvolution peak range and chemical bond assignment.

Band	Peak deconvolution (eV)	Chemical bond
Ti (2p)	455.4 – 456.1	TiN or TiN_xO_y
	457.8 – 458.4	TiO_2
Nb (2p)	203.8 – 204.3	NbN
	207.2 – 207.7	Nb_2O_5
N (1s)	395.7 – 396.5	TiN_{1+x}
	396.9 – 398.0	TiN
	399.5 – 400.0	TiN_xO_y
O (1s)	529.8 – 530.3	TiO_2
	531.8 – 532.6	OH
C (1s)	281.7 – 282.1	TiC
	283.9 – 284.9	C-C or C-H
	285.4 – 286.4	C = O
	287.8 – 288.3	Organic contaminations

Average roughness range, R_a, at two image sizes, of steel substrate and titanium ceramics coatings were determined by AFM from at least three images each, (Table 4).

Roughness is smaller in 10x10 μm^2 images because these images were done in selected smooth regions of the larger images. While in larger images there are craters with hundreds of nanometers height, it is possible to obtain 10x10 μm^2 smooth images without craters.

Table 4 – Average roughness range, R_a, determined by AFM, of steel substrate and titanium ceramic coatings.

Substrate / Image size	10x10 μm²	30x30 μm² or 50x50 μm²
Steel		
not polished	3 – 10	7 – 25
TiN		
not polished	16 – 23	34 – 43
polished	1.2 – 3.2	n.d.
TiNbN		
not polished	8 – 12	22 – 32
polished	1.1 – 1.5	10 – 22
TiCN		
not polished	6 – 25	33 – 61
polished	1.1 – 1.6	7 – 14

These results showed that with the PVD deposition, which resulted in a 2 to 5 μm coating thickness, the surface roughness did not decrease.

Polishing results in a roughness decrease, however, if larger images are considered the roughness decrease is not significant because craters were not eliminated (Figure 2).

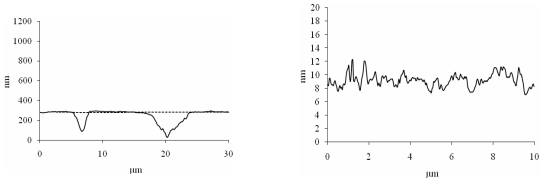

a) b)

Figure 2 – Topographic profile of a polished TiCN coating: a) 30x30μm² and b) 10x10μm².

4.2 Single BSA adsorption

Experimental average adsorptions of BSA on the three titanium ceramics are shown in Figure 3. In the same figure linearization of the Langmuir and Freundlich isotherms is present. It is possible to see that, although Langmuir linearization gives best correlation coefficients, R^2, (see Figure 3a), the experimental results are better approached by Freundlich isotherm (see Figure 3b). Unlike the ideal Langmuir model which is restricted to the formation of a monolayer, the Freundlich isotherm predicts no limit for adsorption. The steady increase of albumin adsorption with concentration observed for the three coatings may be attributed to the formation of a multilayer but it can also be due to the increasing amount of water coupled to the protein film, [24].

In a multilayer system the protein will be weakly attached to the surface and rinsing will drag a significant part of molecules in these conditions. In our case, rinsing led to a very small decrease of the adsorbed mass suggesting the existence of a monolayer.

Although TiN presents slightly higher BSA adsorption the behaviour on the three coatings is quite similar which can be resumed in the several Langmuir and Freundlich isotherm model parameters determined from equations 1 and 2 linearizations (Table 5).

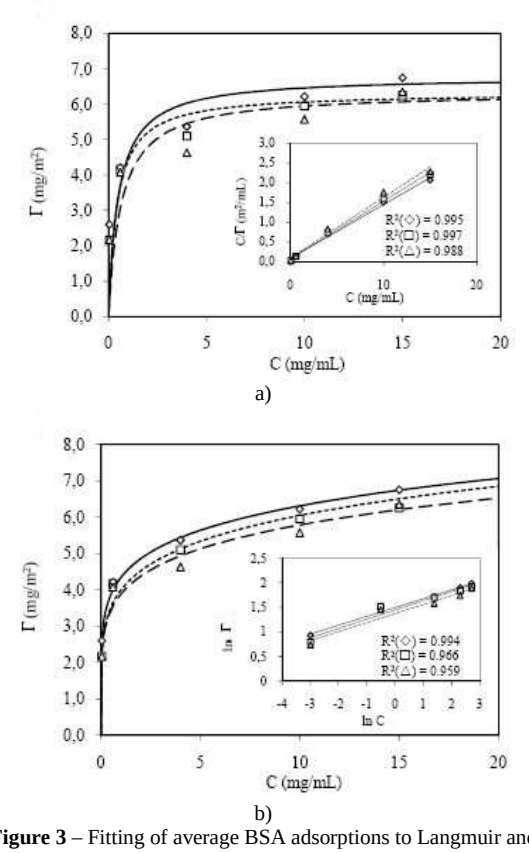

a)

b)

Figure 3 – Fitting of average BSA adsorptions to Langmuir and Freundlich isotherms models in several materials: TiN (full line), TiNbN (dotted line) e TiCN (dashed line). Experimental averages: TiN (diamond), TiNbN (square) e TiCN (triangle). a) Langmuir isotherm and b) Freundlich isotherm.

Table 5 – Adsorption parameters obtained from Langmuir and Freundlich isotherms.

	TiN	TiNbN	TiCN
Γ_∞ (mg/m²)	6.78	6.32	6.33
K_L (L/g)	2.00	2.31	1.56
ΔG_0^{ads} (KJ/mol)	-39.2	-39,6	-38,6
K_F	434	399	388
n_F	6.16	5.56	5.77

Although the average values appear to follow a continuum trend, the BSA adsorption results are very scattered as we can see by the error bars in Figure 4.

In the QCM-D technique the calculated adsorbed mass corresponds to the sum of dry protein and the trapped solvent. If we assume a total mass vs. dry mass ratio of 2.2, [25], the real adsorbed BSA is about 3.0 mg/m². According to some authors, the BSA monolayer superficial concentration limit varies between 1.4 and 3.0 mg/m² for a side-on configuration and between 2.3 and 9.0 mg/m² for a end-on configuration, [3]. Our corrected adsorption mass is in the boundary limit of these two configuration. To known a more exact ratio value the adsorption should be studied by an optical technique like ellipsometry or SPR. With these techniques it is possible to determine the exact protein adsorbed dry mass, [26,27].

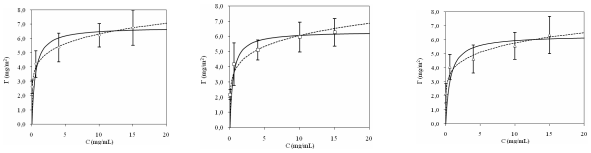

a) b) c)

Figure 4 – Fitting of average BSA adsorptions to Langmuir and Freundlich isotherms models in several materials: a) TiN, b)TiNbN and c) TiCN

The values calculated by Sauerbrey and modified Sauerbrey models are similar with differences up to 7% (usually between 1 and 4%). In the studied conditions, the change of dissipation coefficient, ΔD, are less than 10^{-6} per 5 Hz of Δf. These two results permit us to admit that adsorbed BSA film has a rigid behavior, [28].

Thicknesses, determined by QCM and AFM, of adsorbed BSA layer, from a 10 mg/L BSA solution, are shown in Table 6. Thickness results obtained with QCM technique are averages of at least three analyses. Due to difficulties in the operation of AFM in liquid media, we got only one scratch image for each coating. Thickness values obtained by AFM are influenced by uncertainties such as surface roughness and BSA coverage which lead to a difficulty in assuming a exact baseline (Figure 5). However, values between 3 and 8 nm for the thickness of the protein film were obtained from the AFM scratch experiments. These values are in qualitative agreement with those obtained with the QCM-D technique and are compatible with the molecular dimensions of the BSA molecules (heart-shaped configuration, approximated by an equilateral triangle with side length approximately 8 nm and 3 nm of thickness, [29]) forming an end-on monolayer or a side-on monolayer. The thicknesses obtained by AFM are also in agreement with the ones obtained by Keere *et al* to HSA adsorption in mica and titanium: 4.6 and 3.6 nm respectively, [30].

Table 6 – BSA adsorbed film thickness.

	TiN	TiNbN	TiCN
QCM-D	6.6 ± 0.8	7.6 ± 1.6	5.6 ± 1.0
AFM	3.5†	3.5†	4.9†

† only one topographic profile.

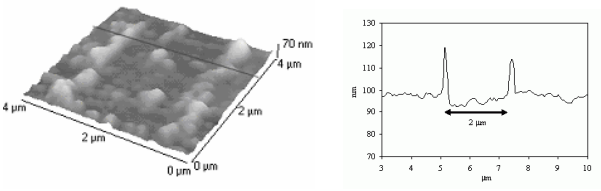

a) b)

Figure 5 – AFM scratch of the BSA film covering a TiNbN coating: a) topographic image of the scratch and b) selected profile.

The comparison of the topographical images, before and after BSA adsorption (Figure 6), allows us to see that the surface features of the bare surface (e.g. polishing scratches) became invisible suggesting that the protein layer covers the whole surface area. Furthermore, the structure of the BSA aggregates can be clearly identified. These aggregates present, in general, a diameter of about 80-150 nm in all the three coatings in agreement with previous studies of Chen *et. al.*, [31].

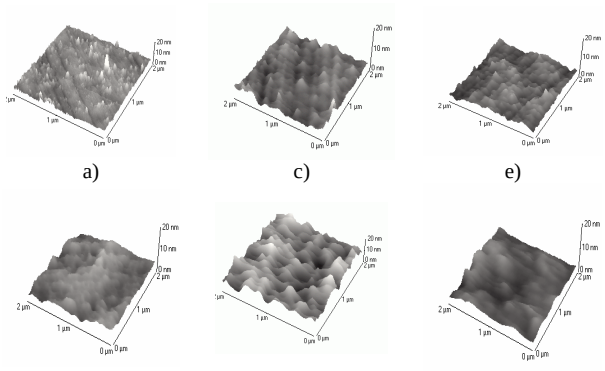

a) c) e)

b) d) f)

Figure 6 – Comparison between substrates topographical images without and with adsorbed BSA: a) TiN without BSA, b) TiN with BSA, c) TiNbN without BSA, d) TiNbN with BSA, e) TiCN without BSA e f)) TiCN with BSA.

4.3 NaHA adsorption (single and combined with BSA)

NaHA adsorption on TiNbN coatings, from a 1 mg/mL solution, results in a superficial concentration of 1.5 ± 0.5 mg/m^2. This is a smaller value compared with the estimated value for BSA adsorption at same solution concentration: ≈ 4 mg/m^2. The studied NaHA concentration is about ¼ of concentration in synovial fluid but if we increase the concentration, the liquid becomes very viscous. Like in the case of BSA adsorption, the experimental values of the adsorption of NaHA are very scattered and the changes of dissipation coefficient, ΔD, are less than 10^{-6} per 5 Hz of Δf.

Sequential tests (NaHA adsorption on the BSA film layer) showed no NaHA adsorption at neutral pH as expected from previous literature, [32,33].

Simultaneous adsorption of NaHA (1 mg/mL) and BSA (10 mg/mL) did not yield significant quantitative change in the adsorbed mass compared to single BSA adsorption, at the same concentration of the solution.

From these three results we can conclude that the interaction between NaHA and BSA is weak and that the adsorption of BSA is faster than the adsorption of NaHA because the presence of NaHA does not affect the value of the mass uptake ($\Gamma_{mixture} \approx \Gamma_{BSA}$).

4.4 Adhesion forces

Experimental adhesion forces in liquid medium (water) were obtained with only one sample analysis for each system. Averages and standard deviations were calculated from 32 and 64 approaching/retracting curves for TiN and TiNbN, respectively, (Table 7).

Our adhesion forces results are not in agreement with previous studies from other authors. Chen *et. al.*, [31], and Hayashi *et. al.*, [34], found that the relative adhesion force order is: surface-Si_3N_4 > surface-BSA > BSA-BSA. However, our experimental results with the TiN coating showed a different order: surface-BSA > BSA-BSA >

surface-Si_3N_4. This difference should be due to the different surface properties of the materials namely the hydrophobicity and the surface charge. While in the above studies polystyrene, [31], and poly-(2-methoxyethyl acrylate) (PMEA), [34], were used, our study reports to titanium ceramics.

Table 7 – Experimental adhesion forces.

	F_{ad} (nN)	
	TiN	**TiNbN**
Surface – Si_3N_4 tip	± 0.10 or less	n.d.
Surface – BSA funcionalized tip	0.67 ± 0.21	0.34 ± 0.05
Surf. with BSA – BSA funcionalized tip	0.56 ± 0.07	0.23 ± 0.03

Another major difference in the referred previous works is the relative surface-BSA adhesion force values. In Hayashi *et. al.* study, [34], the adhesion force between BSA and PMEA surface was 0.06 mN/m and between BSA and poly(n-butyl acrilate) (PBA) was 2.8 mN/m. Sagvolden, [35], measured the adhesion force between BSA and glass and found 30.5 mN/m. In our work we determined 67 and 34 mN/m for the adhesion forces between BSA and TiN and TiNbN, respectively. If Hayashi *et. al.*, [34], considered PBA blood-incompatible due to the high adhesion of BSA, then the titanium ceramics studied (TiN and TiNbN) should be blood incompatible despite their non-citotoxicity, [36].

Van der Waals forces estimated by the Hamaker treatment, F_{VdW}, (Table 8) confirm the decrease in adhesion force when there is BSA on both surfaces, compared with the case where there is only one surface with adsorbed protein. However, these predicted values are much lower than the experimental ones showing us that adhesion is influenced, not only by Van der Walls forces, but also by other forces like electrostatic and hydrophobic interactions. The Hamaker treatment, (equation 12), has also inherent uncertainties like tip radius, interatomic spacing and all the parameters used in the calculation of Hamaker constant.

Table 8 – Theoretical Van der Waals forces.

	F_{vdw} (nN)
TiN – water – Si_3N_4	0.11
TiN – water – BSA	0.05
TiO_2 – water – BSA	0.13
BSA – water – BSA	0.03

5. Conclusions

In this work was studied the adsorption of BSA and NaHA to three titanium nitride coatings which have a high potential to be use in articulating orthopedic prostheses.

Albumin was found to adsorb strongly on the surface of the three coatings. Adsorption isotherms determined with a quartz crystal microbalance have similar shapes, but the mass uptake is slightly higher for TiN.

It was found that sodium hyaluronate adsorbs to the TiNbN coating in smaller quantity than albumin and do not adsorb on the albumin film. These results are in agreement with previous works from other authors.

Our measurements of the adhesion force deviate from the experimental values reported in previous works, specially the ordering of the interactions. However, it should be noted that those results were obtained with polymeric surfaces.

References

[1] Rieker, C.B., Tribology in total hip arthroplasty, Business Briefing: Global Surgery 2003
[2] http://www.genderknee.com (24/09/2008)
[3] Completo, C., Adsorção de albumina bovina e ácido hialurónico em cerâmicos de titânio – Tese de Mestrado; IST; Lisboa, 2008
[4] Liu, C.; Bi, Q.; Matthews, A., Surface and Coatings Technology 2003, 163–164, 597–604
[5] Huang H.-H.; Hsu, C.-H.; Pan, S.-J.; He, J.-L.; Chen, C.-C.; Lee, T.-L., Applied Surface Science, 2005, 244, 253-256
[6] Serro, A.P.; Gispert, M.P.; Martins, M.C.L.; Brogueira, P.; Colaço, R.; Saramago, B., Journal of Biomedical Materials Research Part A 2006, 78 (3), 581-589
[7] Gispert,M.P.; Serro, A.P.; Colaço,R.; Saramago, B., Wear 2006, 260, 149–158
[8] Flannery, M.; Jones, E.; Birkinshaw, C., Wear 2008, 265, 1009-1016
[9] Figueiredo, J.L.; Ribeiro, F.R., Catálise Heterogéna, Fundação Calouste Gulbenkian, 1989
[10] Jackson, D.R.; Omanovic, S.; Roscoe, S.G.; Langmuir 2000, 16, 5449-5457
[11] Rodahl, M.; Höök, F; Fredriksson, C.; Keller, C.A.; Krozer, A.; Brezezinski, P.; Voinova, M.; Kasemo, B. Faraday Discuss. 1997, 107, 229-246
[12] Buck, R.P.; Lindner, E.; Kutner, W.; Inzel, G. Pure Appl. Chem. 2004, Vol. 76, No. 6, 1139–1160
[13] Höök, F.; Kasemo, B.; Nylander, T.; Fant, C.; Sott, K.; Elwing, H. Anal. Chem. 2001, 73, 5796-5804
[14] Kankare, J., Langmuir 2002, 18, 7092-7094 -
[15] Alberty, R.A.; Silbey, J.R, Physical Chemistry, 2nd ed., John Wiley & Sons, 1996
[16] Rough Surfaces, 1st ed., Longman, 1982
[17] Handbook of Micro/Nano Tribology, 2nd ed., CRC Press, 1999
[18] Butt, H.-J.; Cappella, B.; Kappl, M., Surface Science Reports 2005, 59, 1-152
[19] Bertóti, I.; Mohai, M.; Sullivan, J.L.; Saied, S.O., Applied Surface Science 1995, 84, 357-371
[20] Kirchner, C.N.; Hallmeier, K.H.; Szargan, R.; Raschke, T.; Radehaus, C.; Wittstock, G., Electroanalysis 2007, 19(10), 1023–1031
[21] Jouve, G.; Séverac, C.; Cantacuzène, S., Thin Solid Films 1996, 287, 146-153
[22] Dong, Y.-X.; Chen, Y.-S.; Chen, Q.; Liu, B.; Song, Z.-X., Surface & Coatings Technology 2007, 201, 8789–8795
[23] Welle, A.; Chiumiento, A.; Barbucci, R., Biomolecular Engineering 2007, 24, 87–91
[24] Liu. B; Cao, S.; Deng, X.; Li, S.; Luo, R., Appl. Surf. Sci. 2006, 252, 7830–7836
[25] Vörös, J., Biophysical Journal 2004, 87, 553–561
[26] Arwin, H. Thin Solid Films 2000, 377-378, 48-56
[27] Jung, L.; Campbell, C.T.; Chinowsky, T.M.; Mar, M.N.; Yee, S.S Langmuir 1998, 14, 5636-5648
[28] Kaufman, E.D.; Belyea, J.; Johnson, M.C.; Nicholson, Z.M.; Ricks, J.L.; Shah, P.K.; Bayless, M.; Pettersson, T.; Feldotö, Z.; Blomberg, E.; Claesson, P.; Franzen, S., Langmuir 2007, 23, 6053-6062
[29] Kragh-Hansen, U.; Chuang, V.T.G.; Otagiri, M., Biol. Pharm. Bull. 2002, 25(6), 695—704
[30] Van de Keere, I.; Willaert, R.; Tourwé, E.; Hubin, A.; Vereecken, J., Surf. Interface Anal. 2008, 40, 157-161
[31] Chen, X.; Davies, M.C.; Roberts, C.J.; Tendler, S.J.B.; Wolliams, P.M., Langmuir 1997, 13, 4106-4111
[32] Grymonpré, K.R.; Staggemeier, B.A.; Dubin, P.L.; Mattison, K.W., Biomacromolecules 2001, 2, 422-429
[33] Hu, S.-G.; Jou, C.-H.; Yang, M.C., Biomaterials 2003, 24, 2685–2693
[34] Hayashi, T.; Tanaka, M.; Yamamoto, S.; Shimomura, M.; Hara, M., Biointerphases 2007, 2(4), 119-125
[35] Sagvolden, G., Biophysical Journal 1999, 77, 526-532
[36] Serro, A.P.; Completo, C.; Colaço,R.; Santos, F.; Silva, C.L.; Cabral, J.M.S.; Araújo, H.; Pires, E.; Alves, E.; Saramago, B., A comparative study of titanium nitrides, TiN, TiNbN and TiCN, as coatings for biomedical applications, (submited)